EXPERIMENTAL ANALYSIS AND COMPUTATIONAL FLUID DYNAMICS SIMULATIONS FOR HEAT TRANSFER IN SOUND ASSISTED FLUIDIZED BED OF FINE POWDERS

by

Uday WANKHEDE [a*] ***and Ram SONOLIKAR*** [b]

[a] G. H. Raisoni College of Engineering, Nagpur, Maharashtra, India
[b] Laxminarayan Institute of Technology, Nagpur, Maharashtra, India

Original scientific paper
https://doi.org/10.2298/TSCI150208124W

Fine powders in the size range of 20-200 μm are widely used in industries for fluid bed operations and are ideal for gas-solid reactions because of their large external surface areas and favorable heat transfer rates. The fine powders have very poor flow characteristics. Most of the earlier research work in heat transfer in bubbling fluidized beds is focused on coarse grained Geldart B and D particles. Acoustic energy of sufficient intensity and sound pressure level improved the quality of fluidization of fine powders. The objective of this investigation is experimental analysis and CFD simulations for heat transfer in a fluidized bed of fine powders at different acoustic conditions. The Eulerian approach has been identified as an efficient method for the numerical simulation of fluidized beds. The experimental and CFD results are in good agreement with each other.

Key words: *fluidization, heat transfer, acoustics, CFD*

Introduction

Due to high cost and more time consuming experimentation on fluidization, more researchers are extending their efforts towards developing the mathematical model and numerical simulation with the help CFD and validating the experimental results with CFD results. It is possible to study large number of parameters in stipulated time and develop the optimized solution to work. There are two approaches for CFD modelling of gas-solid flows: Eulerian – Eulerian model and Eulerian – Lagrangian models. In the current work, experimental analysis and numerical simulation for the heat transfer between a fluidized bed and immersed heat transfer surface in the absence and presence of acoustic waves is of particular interest.

The heat transfer coefficients were estimated numerically by Karamavruc *et al*. [1] from governing heat conduction equations using both 1-D and 2-D analysis. The analysis showed that temperature gradient existed around the tube which led to different heat transfer coefficients for 1-D and 2-D cases. At velocities close to minimum fluidization velocity, the instantaneous heat transfer coefficient showed considerable difference. At higher gas velocities, the increase in bubble frequency resulted in decrease in temperature gradients around the circumference of the tube. This led to difference in heat transfer coefficients. Kuipers *et al*. [2] developed a computer model for a hot gas fluidized bed. They used two fluid model (TFM) approach in which both the phases were considered to be continuous and fully interpenetrating. Local wall-to-bed heat transfer coefficients were estimated by the simultaneous solution of the TFM conservation of mass, momentum, and thermal energy equations.

* Corresponding author, e-mail: udaywankhede74@gmail.com

The effects of acoustic vibrations on minimum fluidization velocity, bed characteristics, and heat transfer rates with particle sized from 7-97 μm in a fluidized bed were reported by Nowak *et al*., [3]. It was found that acoustic energy at low frequency significantly improved the quality of fluidization of non-fluent materials. Maximum effect on heat transfer rates was observed at acoustic resonance. Chirone *et al*. [4] developed a theory of model cluster breakage. The break-up of clusters occurred at contact points where the external forces induced by acoustic fields were larger than the internal Van der Waals forces. They explained the influence of particle size and surface geometry on the detachment of subclusters from clusters.

Sunderesan and Clark [5] carried out experiments with fluidized bed at ambient conditions and tube containing steam at 100 ºC for glass beads of size 467 μm. They carried out experiments at different bed heights and fluidizing velocities and reported higher time averaged values of heat transfer coefficients for higher gas velocities. Miyamoto *et al*. [6] studied particle contact heat transfer augmentation mechanisms. Conditional averaging statistical analysis was done by distinguishing the measured results between the periods of particle contact and no particle contact.

Levy [7] studied the effect of sound pressure level (SPL) and sound frequency on minimum fluidization velocity. At natural frequency of the bed, high intensity sound waves resulted in reductions in both minimum bubbling and minimum fluidization velocities. Various physical models needed to give an Eulerian formulation of the particulate enthalpy equations were formulated by Schmidt and Renz [8]. The experimentation to measure the thickness of the gas-gap was performed by Huang and Levy [9].They used fiber optic probe for measurement of gas film thickness. The gas-gap thickness was found to depend strongly on angular position around the surface of horizontal tube and the powder properties and to vary slightly with SPL and superficial air velocity.

Wang *et al*. [10] concluded that for particles with $d_p > 0.8$ mm, the effects of thermophysical properties of particles on heat transfer coefficient become important with particle diameter decreasing. For particles with $d_p \leq 0.8$ mm, the effects of the properties on heat transfer were limited. For all particles in the range 0.35-1.21 mm, the heat transfer coefficient between fluidized bed and immersed surfaces was insensitive to particle thermal conductivity.

Numerical analysis of the heat transfer between a bubbling fluidized bed of monodispersed glass beads of group B type and an immersed heater tube was studied by Schmidt and Renz [11]. An Eulerian approach was used for the solution of the mass, momentum, and energy equations of both phases. Various physical models were used for thermal transport coefficient of the solid phase. The fluidization behavior of fine cohesive powders in acoustic field was investigated by Guo *et al.* [12]. The increase in SPL led to reduction in minimum fluidization velocity. The fluidization quality of fine powders improved with increase in SPL. It was found that sound wave configurations influence the fluidization process of fine powders. Natale *et al*. [13] used an interpretative model, based on dimensional analysis, for the description of the experimental results. They reported that the heat transfer coefficients could be improved by using heating surfaces with aerodynamic shapes.

The gas flow and heat transfer between fluidized beds and the surfaces of an immersed object was numerically simulated by Gao *et al*. [14] with the help of a double particle-layer and porous medium model. The dynamic characteristics of the gas phase, the temperature change of particles and the radiative parameters of a particle group were estimated by them. Natale *et al*. [15] studied effect of pressure, temperature and bed material properties on the heat transfer coefficients in fluidized beds. The use of appropriate small proportions of inert Group A particles resulted in improving the fluidization quality of nanopowders as compared to the use of acoustic energy [16].

The investigations for heat transfer for different sized particles at different acoustic conditions, gas velocities, and angular positions around the circumference of heat transfer surface were carried out [17]. The optimum fluidization velocities and acoustic conditions for better heat transfer rates from the surface to the bed material were found out. Acoustic energy of appropriate intensity and sound pressure level significantly improved the quality of fluidization of fine powders. The effects caused by sound wave frequency and sound pressure level on the minimum fluidization velocity in a 3-D fluidized bed was investigated [18]. With increase in acoustic frequency, the minimum fluidization velocity decreased until a specific frequency was reached. Beyond this, the minimum fluidization velocity was found to increase.

Experimental set-up for sound assisted fluidized bed

Figure 1 shows the experimental set-up for heat transfer in a sound assisted fluidized bed. The fluidized bed is an 11.5 cm acrylic column with 61 cm height. The digital signal generator was used to vary acoustic frequency. The loudspeaker generated acoustic waves during experimentation. The microphone Bruel and Kjaer make was used to measure SPL. The output of microphone was processed with digital storage oscilloscope. An electrical heater composed of a tube 2.5 cm diameter and 11 cm length was used to determine the convective heat transfer coefficient. Teflon bushes were used on both sides of tube to minimize heat losses. Figure 2 shows arrangement of thermocouples on the heat transfer tube. It is mounted horizontally with its center axis 80 mm above the distributor. Temperatures were recorded at four distinct locations at an angle of 90° along the circumference of heat transfer tube.

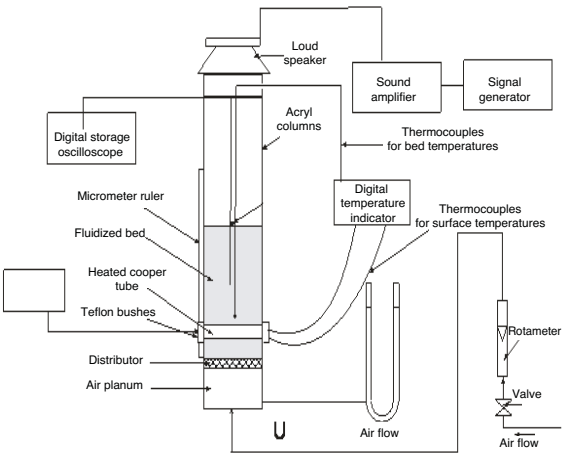

Figure 1. Schematic for experimental set-up of sound assisted fluidized bed apparatus

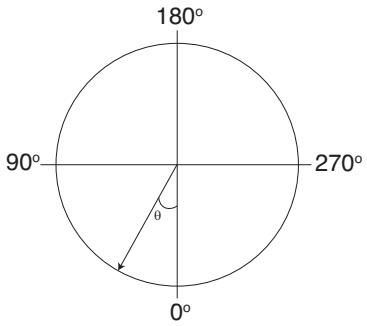

Figure 2. Schematic for location of thermocouples on heat transfer tube

Fluidization behavior and heat transfer in fluidized bed for silica gel with and without sound conditions

Table 1 summarizes the properties of the fluidized bed material and fluidizing agent (air) at standard conditions. Summary of test conditions for heat transfer measurements of fine powder is given in tab. 2.

Table 1. Properties of the fluidized bed materials and fluidizing agent at standard conditions

Bed material	d_p [μm]	C_P [JKg^{-1}-K^{-1}]	k_P [$Wm^{-1}K^{-1}$]	ρ_p [Kgm^{-3}]
Silica gel	25	810	1.9	2300
Air (fluidizing agent)	–	1005	0.0263	1.205

Table 2. Summary of test conditions for heat transfer measurements of fine powder

Bed materials	d_p [μm]	Range of u_g-u_{mf} [cms^{-1}]	Range of u/u_{mf}	Acoustic conditions	
				Acoustic frequency [Hz]	*SPL* [dB]
Silica gel	25	0.2-8.8	1.2-8.4	90	108,112,120,125,130,136, 140,144, without sound

Variation of surface temperature with angular position around circumference of the tube

Figures 3 and 4 show the variation of surface temperature with angular positions for silica gel (25 μm) at conditions of no sound and 140 dB. It was evident that at the beginning of the particle movement *i. e*. at the onset of fluidization and bubbling conditions up to gas velocity of 4.7 cm/s (u_g/u_{mf} = 3.9), the lowest values of surface temperatures were recorded at the lateral sides of the tube for all conditions of no sound and with sound. This behavior can be attributed to the vigorous particle motion in these zones. On the other hand, larger values of surface temperatures were recorded at the frontal and after zones of the heater.

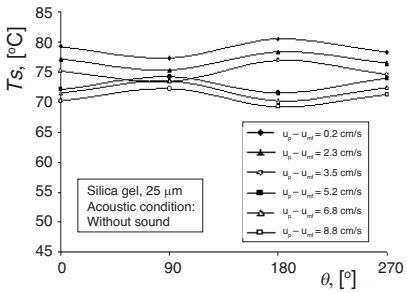

Figure 3. Variation of surface temperature with angular position around circumference of the tube for silica gel (25 μm), Q = 8 W, L/D = 1, without sound

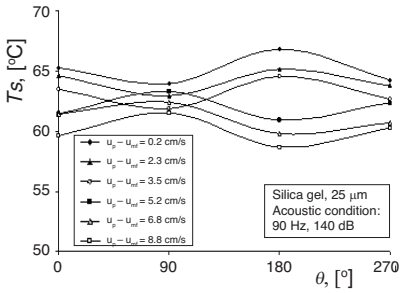

Figure 4. Variation of surface temperature with angular position around circumference of the tube for silica gel (25 μm), Q = 8W, L/D = 1, 140 dB

The highest values of surface temperatures were noted at the top position of the thermocouple (θ = 180°). As the fluid velocity gradually increased beyond 4.7 cm/s (u_g/u_{mf} = 3.9) up to a value of 10 cm/s (u_g/u_{mf} = 8.4), the bed passed from the bubbling regime to the turbulent mixing regime. The value of surface temperature decreased, as a result of bed expansion, and the consequent decrease in the solids concentration. Furthermore, at these high gas velocities, the location for values of maximum surface temperatures shifted to the sides of the tube and minimum surface temperature shifted to the top position (θ = 180°) due to the intensive mixing at top position for all acoustic conditions. The variation in surface temperatures at θ = 180° is affected by the bubble motion, together with sliding motion of particles at side location of the tube. At the top of the tube, the variation of the surface temperature with time is minimal as compared to other locations.

Variation of local heat transfer coefficients

Figures 5 and 6 show variation of local heat transfer coefficients with excess air velocity (u_g-u_{mf}) at different values of θ and figs. 7 and 8 show variation of local heat transfer coefficients with angular position at different values of excess air velocity (u_g-u_{mf}) for silica gel

(25 μm) for no sound and 140 dB, respectively. For initial conditions, for u_g/u_{mf} up to 3.9, the location for maximum local heat transfer coefficients was at the sides of the tube. With increase in gas velocity up to $u_g/u_{mf} = 3.9$, the local heat transfer coefficient increased due to increasing replacement of packets of particles at the tube surface. The values of local heat transfer coefficients were higher for the bottom positions than for the top positions on the tube. With further increase in gas velocity beyond $u_g/u_{mf} = 3.9$, it was found that the values of local heat transfer coefficients reduced for all conditions of SPL. The values of local heat transfer coefficients improved in the SPL range 112-140 dB.

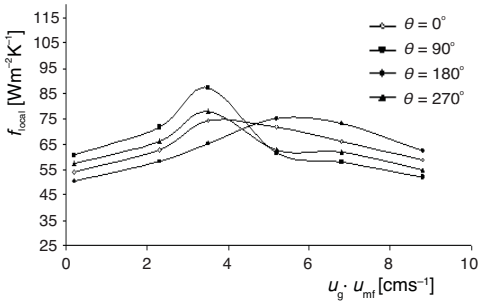

Figure 5. Variation of local heat transfer coefficients with excess air velocity (u_g-u_{mf}) at different values of θ for silica gel (25 μm), Q = 8 W, L/D = 1, without sound

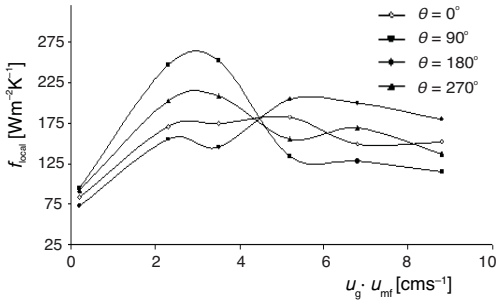

Figure 6. Variation of local heat transfer coefficients with excess air velocity (u_g-u_{mf}) at different values of θ for silica gel (25 μm), Q = 8 W, L/D = 1, 140 dB

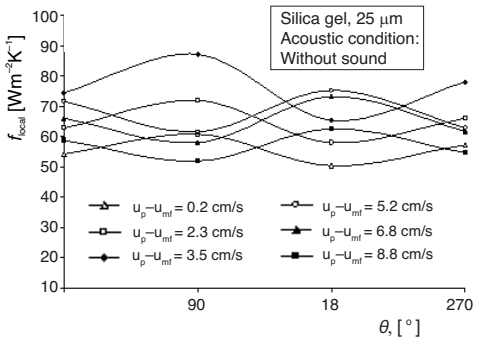

Figure 7. Variation of local heat transfer coefficients with angular position (θ) at different values of excess air velocity (u_g-u_{mf}) for silica gel (25 μm), Q = 8 W, L/D = 1, without sound

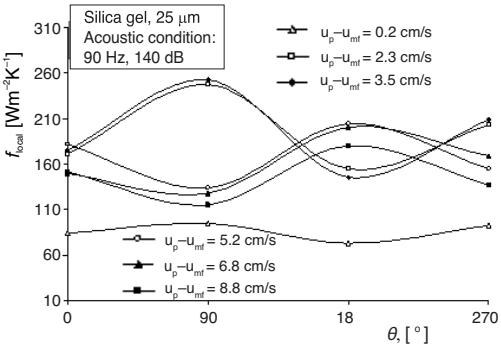

Figure 8. Variation of local heat transfer coefficients with angular position (θ) at different values of excess air velocity (u_g-u_{mf}) for silica gel (25 μm), Q = 8 W, L/D = 1, 140 dB

It can be concluded that at minimum fluidization and bubbling conditions, the position for maximum value of local heat transfer coefficients was located at the sides of the tube. However, with further increase in gas velocity, the position of maximum value of local heat transfer coefficients shifted towards the rear (θ = 180°). The high value of local heat transfer coefficients was obtained at the boundary between bubbling state and turbulent state. The particle motions adjacent to the tube have a direct relation with bubble motion that may affect heat transfer in the bed. The local heat transfer coefficients were found to reduce after 140 dB up to 144 dB. This was attributed to very high momentum and very little time available for the fine powder particles at high sound intensity to receive heat from the heat transfer surface and transmit it to the bed material.

The heat transfer rate between a heat exchanger tube and a fluidized bed depend upon the particle concentration close to the heat transfer surface and particle residence times at the tube surface. The larger values of local heat transfer coefficients were obtained with shorter residence time of the fine powder particles or packets with solid hold-ups. The particle residence time on the tube surface depend on the frequency of replacement of solid packets by bubbles. For gas velocities up to $u_g/u_{mf} = 3.9$, the local heat transfer coefficient values were low since solid particles resided longer on top of the tube with lower bubble frequencies. In the side region of the tube, the local heat transfer coefficient values were higher due to short residence time with vigorous bubbling having high frequency in spite of lower emulsion fractions or solid hold-ups. The high values of local heat transfer coefficients at sides were attributed to short residence time of emulsion phase due to bubbles rising from the tube bottom and sliding of particles from top section of the tube, which resulted in vigorous solids mixing having comparatively higher solid holdups. The emulsion contacting time decreased with increase in gas velocity, due to increase in bubble frequency for gas velocities up to $u_g/u_{mf} = 3.9$, which resulted in higher surface renewal rates with higher solids mixing and consequent increase in local heat transfer coefficients. This situation was reversed for gas velocities beyond u_g/u_{mf} of 3.9.

Variation of average heat transfer coefficients

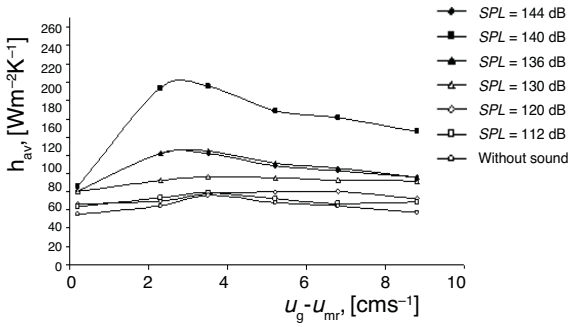

Figure 9. Variation of average heat transfer coefficients *vs* excess air velocity (u_g-u_{mf}) at different SPL for silica gel (25 µm), Q = 8 W, L/D = 1

Figure 9 shows the effect of gas velocity for different acoustic conditions. The average heat transfer coefficient increased appreciably from low SPL values of 112 dB. The range of average heat transfer coefficient was found out to be 55.69 W/m^{2}K at no sound condition to 195.49 W/m^{2}K at 140 dB and gas velocity of 4.7 cm/s. For all conditions of SPL, the values of average heat transfer coefficient increased up to gas velocities of $u_g/u_{mf} = 3.9$. However, with further increase in gas velocity up to $u_g/u_{mf} = 8.4$, the value of average heat transfer coefficient reduced.

Otimal fluidization velocity and optimal SPL

For almost all acoustic conditions used in experimentation, it was evident that the heat transfer coefficient increases with increased in the value of superficial gas velocity. The rate of increase was larger in the beginning but decreased as the fluidizing velocity was increased. The heat transfer coefficient attained maximum value at optimum gas velocity. With further increase in gas velocity, the value of heat transfer coefficient decreased. The heat transfer rate between an immersed surface and the gas solid fluidized bed of small particles mainly depends on particle concentration close to the heat transfer surface and the particle residence time at the heat transfer surface. The particle residence time depends on the solids mixing which is due to rising bubbles. The initial rise in heat transfer coefficient was mainly due to a lowering of particle residence time, thus from greater particle mixing. The large degree of mixing was due to high bubble frequency resulting from a large gas velocity. However, the bulk particle packing density decreased with increase in gas velocity which causes a reduction in heat transfer rate.

Acoustic waves with high intensity (130-144 dB) caused the fine particles to oscillate with the sound waves. The pressure oscillations of both fluidizing gas and the fine particles should be of the same order. Under these circumstances, due to increased motion of fine particles, the adhesion force reduced and the bed began to expand and fluidize when fluidizing air was passed through the column. However, increased motion of fine particles led to higher collisions between particles resulting in their agglomeration. Hence, only optimum and sufficient acoustic energy is needed for avoiding particles against bonding together.

Maximum heat transfer at sides of heat transfer surface

At the low gas velocities, the maximum local heat transfer coefficients were obtained at a place at the sides of the heat transfer tube ($\theta = 90^{o}$ and $\theta = 270^{o}$) due to intensive particle circulation while the minimum heat transfer coefficients were obtained on the upstream side of the tube. The low values of local heat transfer coefficients on the upstream side were due to presence of stagnant caps of defluidized solid particles. The heat transfer in the bed showed results that varied at different angular positions around the tube because the contact behaviors of the emulsion phase with the tube wall were not the same at all angular positions. The location for maximum local heat transfer coefficient moved from the sides of the heat transfer tube to the topmost position on the heat transfer surface. At higher gas velocities, the bed porosity close to the tube increased significantly at the sides of the tube, whereas at the topmost position of the tube($\theta = 180^{o}$), the bed density was relatively high because of moving caps of solid particles.

Governing equations

The Eulerian CFD model used in this work is based on TFM in which both the solids phase and gas phase are treated as continuous. In this work, the drag function of Gidaspow and Shyamlal [19] is used for calculations of drag force. The solid phase properties *i. e.* solid pressure and solid viscosity are calculated with the help of kinetic theory of granular flows. For the interphase heat exchange in the thermal energy equation, the expression from Gunn and Hilal [19], (1996) has been used. The thermal conductivity of particle material differs from that of the particulate phase depending on the contacts of the particles in the fluidized beds and these values are calculated from the correlations proposed by Shyamlal and Gidaspow [20].

Mass balance equations

Equations (1) and (2) express mass balance equations for both gas and solid phase, respectively.

Gas phase:

$$\frac{\partial}{\partial t}\left(\varepsilon_g \rho_g\right) + \nabla\left(\varepsilon_g \rho_g \upsilon_g\right) = 0 \tag{1}$$

Solid phase:

$$\frac{\partial}{\partial t}\left(\varepsilon_s \rho_s\right) + \nabla\left(\varepsilon_s \rho_s \upsilon_s\right) = 0 \tag{2}$$

Momentum balance equations

Equations (3) and (4) are momentum balance equations for both gas and solid phase, respectively. In the gas-solid multiphase flow system, the net force includes viscous force, body force, solid pressure force, and interphase force, which couples the gas and solid momentum equations by drag forces.

Gas phase:

$$\frac{\partial}{\partial t}\left(\varepsilon_g \rho_g \upsilon_g\right) + \nabla\left(\varepsilon_g \rho_g \upsilon_g \upsilon_g\right) = \nabla \tau_g - \varepsilon_g \nabla p + \varepsilon_g \rho_g g - \beta\left(\upsilon_g - \upsilon_s\right) \tag{3}$$

Solid phase:

$$\frac{\partial}{\partial t}\left(\varepsilon_s \rho_s \upsilon_s\right) + \nabla\left(\varepsilon_s \rho_s \upsilon_s \upsilon_s\right) = \nabla \tau_s - \nabla p_s^* - \varepsilon_s \nabla p + \varepsilon_s \rho_s g - \beta\left(\upsilon_s - \upsilon_g\right) \tag{4}$$

Energy balance equations

Equations (5) and (6) are energy balance equations for both gas and solid phase, respectively. Equation (7) represents equations for enthalpy and heat exchange between gas and solid phase, respectively. The enthalpy equations are required for the thermal conduction within the phase, the heat exchange between the gas and solid phase and the viscous dissipation and the term involving the work of expansion of the void fraction.

Gas phase:

$$\frac{\partial}{\partial t}\left(\varepsilon_g \rho_g h_g\right) + \nabla\left(\varepsilon_g \rho_g h_g \upsilon_g\right) = -\nabla \varepsilon_g q_g + \alpha\left(T_s - T_g\right) + \tau_g \nabla \upsilon_g + \varepsilon_g \left[\frac{\partial}{\partial t} p + \upsilon_g \nabla p\right] \tag{5}$$

Solid phase:

$$\frac{\partial}{\partial t}\left(\varepsilon_s \rho_s h_s\right) + \nabla\left(\varepsilon_s \rho_s h_s \upsilon_s\right) = -\nabla \varepsilon_s q_s + \alpha\left(T_g - T_s\right) + \tau_s \nabla \upsilon_s + \varepsilon_s \left[\frac{\partial}{\partial t} p + \upsilon_s \nabla p\right] \tag{6}$$

$$h_i = \int_{T_{\text{ref}}}^{T} c_{p,i}\, \mathrm{d}T_i \text{ and } q_i = -k_i \nabla T_i \tag{7}$$

Gunn model

Equation (8) express Gunn model for estimation of Nusselt number. The correlation of Gunn model [19] for heat exchange is valid for a wide range of particle volume fractions, so that its application on the simulation of bubbling fluidized beds is reasonable, as particle volume fraction ranges from 0 to 0.6.

$$\mathrm{Nu} = \frac{\alpha_{gs} d_g}{k_g} = \left(7 - 10\varepsilon_g + 5\varepsilon_g^2\right)\left(1 + 0.7\,\mathrm{Re}^{0.2}\,\mathrm{Pr}^{1/3}\right) + \left(1.33 - 2.4\varepsilon_g + 1.2\varepsilon_g^2\right)\mathrm{Re}^{0.7}\,\mathrm{Pr}^{1/3} \tag{8}$$

Computational model

The bubbling fluidized bed simulations were performed using FLUENT, a commercial finite volume code. The air was supplied from the lower end of the tube through the distributor for uniform distribution. The variable flow rate of air gave variation in the air velocity at the inlet of tube. The fluidization velocity for the simulations was in the same range as that for the experimental findings. The pressure at the outlet was considered as atmospheric pressure. The 3-D double precision segregated, unsteady, first order implicit, Eulerian solver was considered for simulation. Table 3 summarizes the system initial conditions for silica gel (25 μm) at heat input of 8 W, *L*/*D* ratio of 1 and without sound conditions. The system initial conditions for silica gel (25 μm) at heat input of 8 W, *L*/*D* ratio of 1 and 140 dB are summarized in tab. 4.

Table 3. System initial conditions for silica gel (25 µm) at Q = 8 W, L/D = 1, without sound conditions

Initial bed height [m]	0.115
Bed diameter [m]	0.115
Gas velocity [cms^{-1}]	1.4,3.5,4.7,6.4,8,10
Minimum fluidization velocity [cms^{-1}]	1.2
Heat input to heater [W]	8
Initial bed temperature [K]	300
Acoustic condition [B]	Without sound

Table 4. System initial conditions for silica gel (25 µm) at Q = 8 W, L/D = 1,140 dB

Initial bed height [m]	0.115
Bed diameter [m]	0.115
Gas velocity [cms^{-1}]	1.4,3.5,4.7,6.4,8,10
Minimum fluidization velocity [cms^{-1}]	1.2
Heat input to heater [W]	8
Initial bed temperature [K]	300
Acoustic condition [dB]	140

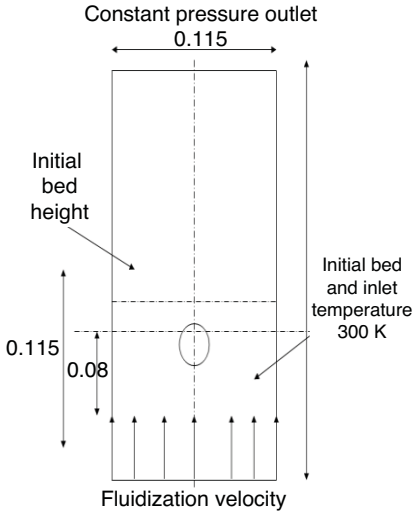

Figure 10. Sketch of numerical setup (L/D = 1); (all dimensions are in meters)

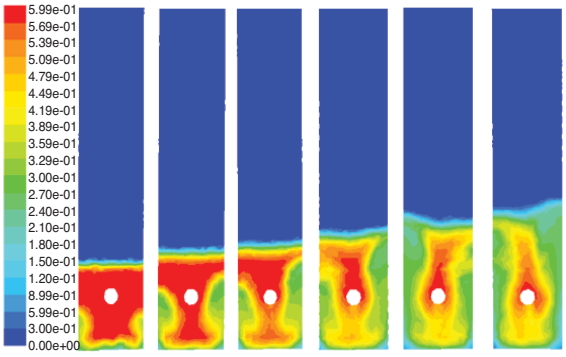

Figure 11. Contours of solid volume fractions at different fluidization velocities for silica gel (25 µm) at 8 W, L/D = 1, without sound condition

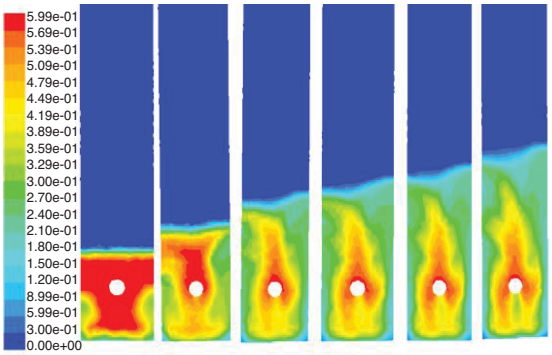

Figure 12. Contours of Solid Volume Fractions at different fluidization velocities for silica gel (25 µm) at 8 W L/D = 1, 140 dB

Figure 10 show numerical set-up for simulation work. Figures 11 and 12 show the contours of solid volume fractions at different fluidization velocities for silica gel (25 µm) at 8 W, L/D = 1, without sound condition and at 140 dB, respectively. Figures 13 and 14 show comparison of experimental and simulation results of silica gel (25 µm) at 8 W, L/D = 1, without sound condition and at 140 dB, respectively. It is clear from these figures that the average heat transfer coefficients for both conditions of no sound and with sound were good agreement with experimental findings.

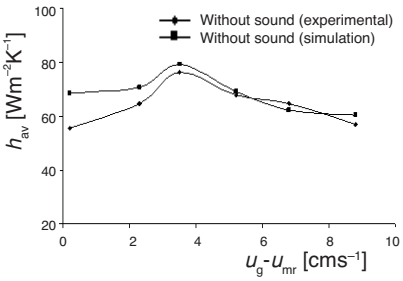

Figure 13. Comparison of experimental and simulation results of silica gel (25 µm) at 8 W, *L/D* = 1, without sound condition

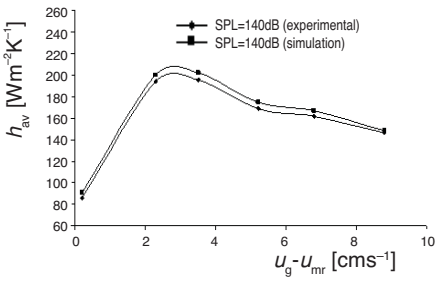

Figure 14. Comparison of experimental and simulation results of silica gel (25 µm) at 8 W, *L/D* = 1, 140 dB

Conclusions

The fluidization of fine, sticky Geldart group C and A powders were very difficult. Acoustic waves with sufficiently high amplitude and low frequency improved the quality of fluidization and hence heat transfer rates appreciably. Heat transfer rates increased sharply up to gas velocities 2-3 times the minimum fluidization velocity. It reached a maximum value at some optimal fluidization velocity. With further increase in fluidization velocity, heat transfer intensity by the immersed surfaces decreased. In the range of velocities lower than the optimal, the key mechanism was particle convection, the intensity of which increased with the increase in particle mixing. For fluidization velocities higher than the optimal, the key mechanism of heat transfer was gas convection. Due to low fluidized bed density in this range of velocities, influence of heat transfer by particle convection decreased. This trend was evident in the fine powders for which the gas velocities used were of the order of 6-9 times the minimum fluidization velocity.

Eulerian approach has been identified as most suitable approach for fluid dynamics and heat transfer in fluidized beds. Heat transfer coefficient has strong influence with rising bubbles near wall of heated pipe. Heat transfer coefficient increased drastically for higher velocities in presence of acoustic waves. The numerical tool was able to explain and predict the flow dynamics and heat transfer in fluidized beds of fine powders of group C and A both without and with sound assistance. The average heat transfer coefficients for both conditions of no sound and with sound were in good agreement with experimental findings.

Nomenclature

A_S – surface area of the heater, [m^2]
C_d – specific heat of emulsion phase, [Jkg^{-1}K^{-1}]
C_g – specific heat of gas, [Jkg^{-1}K^{-1}]
C_p – specific heat of solid particle, [Jkg^{-1}K^{-1}]
D – bed diameter, [m]
d_p – particle diameter, [m]
f – frequency of sound waves, [Hz]
H – bed depth, [m]
h – convective heat transfer coefficient in the fluidized bed, [Wm^{-2}K^{-1}]
h_{av} – average heat transfer coefficient, [Wm^{-2}K^{-1}]
h_b – convective heat transfer coefficient for emulsion (dense) phase, [Wm^{-2}K^{-1}]
h_d – convective heat transfer coefficient for bubble phase, [Wm^{-2}K^{-1}]
h_{local} – local heat transfer coefficient, [Wm^{-2}K^{-1}]
h_{max} – maximum heat transfer coefficient, [Wm^{-2}K^{-1}]
h_r – radiation heat transfer coefficient, [Wm^{-2}K^{-1}]
I – current, [A]
L – initial bed height, [m]
P_e – effective pressure of sound wave, [Pa]
P_o – reference pressure of sound wave at standard condition, (=2·10^{-5} Pa)
p – acoustic pressure at any point
Q – heat generation, [W]

SPL – sound pressure level, [dB]
U_{opt} – optimum superficial gas velocity, [cms^{-1}]
u – velocity, [cms^{-1}]
u_{mb} – minimum bubbling velocity, [cms^{-1}]
u_{mf} – minimum fluidization velocity, [cms^{-1}]
u_g – superficial gas velocity, [cms^{-1}]
u_g-u_{mf} – excess air velocity, [cms^{-1}]
V – voltage, [volts]

Greek symbols

ε – void fraction of the emulsion (dense) phase
θ – angular position around the tube, measured clockwise from the bottom of the tube
μ – viscosity, [kg s^{-1}m^{-1}]
ρ_g – gas density, [kgm^{-3}]
ρ_p – particle density, [kgm^{-3}]

References

[1] Karamavruc, A., *et al*., Deduction of Fluid Bed Heat Transfer Coefficients Using One and Two Dimensional Analysis, *Powder Technology*, *80* (1984), 1, pp. 83-91
[2] Kuipers, J., *et al*., Numerical Calculation of Wall-to-Bed Heat Transfer Coefficients in Gas-Fluidized Beds, *AIChE*, *32* (1992), 7, pp. 1079-1091
[3] Nowak, W., *et al*., Fluidization and Heat Transfer in an Acoustic Field, *AIChE Symposium Series*, *89* (1993), 296, pp. 137-149
[4] Chirone, R., *et al*., Bubble-Free Fluidization of a Cohesive Powder in an Acoustic Field, *Chemical Engineering Science*, *48* (1993), 1, pp. 41-51
[5] Sunderesan, R., Clark, N. N., Local Heat Transfer Coefficients on the Circumference of a Tube in a Gas Fluidized Bed, *International Journal of Multiphase Flow*, *21* (1995), 6, pp. 1003-1024
[6] Miyamoto, M., *et al*., Unsteady Heat Transfer and Particle Behavior around a Horizontal Tube Bundle Near an Expanded Bed Surface of a Gas Fluidized Bed-Conditional Sampling Statistical Analysis, *International Journal of Heat and Mass Transfer*, *38* (1995), 17, pp. 3263-3273
[7] Levy, E., Bubbling Fluidization of Fine Powders in a High Intensity Acoustic Field, *Proceedings,* International Fluidization Conference, Durango, Col., USA, 1998
[8] Schmidt, A., Renz, U., Eulerian Computation of Heat Transfer in Fluidized Beds, *Chemical Engineering Science*, *54* (1999), 22, pp. 5515-5522
[9] Huang, D., Levy, E., Gas Gap at the Surface of a Horizontal Tube in a Bubbling Fluidized Bed, *Powder Technology*, *140* (2004), 1-2, pp. 131-135
[10] Wang, L., *et al*., Effects of Solid Particle Properties on Heat Transfer between High Temperature Gas Fluidized Bed and Immersed Surface, *Applied Thermal Engineering*, *24* (2004), 14-15, pp. 2145-2156
[11] Schmidt, A., Renz, U., Numerical Prediction of Heat Transfer between a Bubbling Fluidized Bed and an Immersed Tube Bundle, *Heat Mass Transfer*, *41* (2005), 3, pp. 257-270
[12] Guo, Q., *et al*., Influence of Sound Wave Characteristics on Fluidization Behaviors of Ultrafine Particles, *Chemical Engineering Journal*, *119* (2006), 1, pp. 1-9
[13] Natale, F. D., *et al*., Surface-to-Bed Heat Transfer in Fluidized Beds: Effect of Surface Shape, *Powder Technology*, *174* (2007), 3, pp. 75-81
[14] Gao, W. M., *et al*., Computational Simulation of Gas Flow and Heat Transfer Near an Immersed Object in Fluidized Beds, *Advances in Engineering Software*, *38* (2007), 11-12, pp. 826-834
[15] Natale, F. D., *et al*., A Single Particle Model for Surface-to-Bed Heat Transfer in Fluidized Beds, *Powder Technology*, *187* (2008), 1, pp. 68-78
[16] Wankhede, U. S., *et al*., Effect of Acoustic Field on Heat Transfer in a Sound Assisted Fluidized Bed of Fine Powders, *International Journal of Multiphase Flow*, *37* (2011), 9, pp. 1227-1234
[17] Escudero, D. R., Acoustic Field Effects on Minimum Fluidization Velocity in a 3D Fluidized Bed, *Proceedings,* Graduate Research Symposium, Iowa State University, Ames, La., USA, 2012
[18] Ajbar, A., *et al*., Fluidization of Nano-Powders: Effect of Sound Vibration and Pre-Mixing with Group A Particles, *Powder Technology*, *206* (2011), 3, pp. 327-337
[19] Gunn, D. J., Hilal, N., Heat Transfer from Vertical Inserts in Gas-Fluidized Beds, *Int. J. Heat Mass Transfer*, *39* (1996), 16, pp. 3357-3365
[20] Syamlal, M., Gidaspow, D., Hydrodynamic of Fluidization: Prediction of Wall to Bed Heat Transfer Coefficients, *AlChE Journal*, *31*, (1985), 1, pp. 127-135

Paper submitted: February 8, 2015
Paper revised: August 6, 2015
Paper accepted: August 6, 2015